RAPID, TIME-RESOLVED PROXIMITY LABELING BY SBP1 IDENTIFIES A PORIN DOMAIN PROTEIN AT THE MALARIA PARASITE PERIPHERY

David Anaguano[1,2], Carrie F. Brooks[2], David W. Cobb[1,2,#], and Vasant Muralidharan[1,2,*]

[1]Department of Cellular Biology, [2]Center for Tropical and Emerging Global Diseases, University of Georgia, Athens, GA

[#]Current address: Department of Microbiology and Immunology, Vagelos College of Physicians and Surgeons, Columbia University, New York, NY

[*]Corresponding author: vasant@uga.edu

ABSTRACT

The deadly human malaria-causing parasite, *Plasmodium falciparum* relies on its capacity to completely remodel its host red blood cell (RBC) through the export of several hundred parasite proteins across several membranes to the RBC. Among these exported proteins are several membrane proteins that are assumed to be inserted into the parasite plasma membrane (PPM) during their transport via the secretory pathway. It is not known how these exported membrane proteins are extracted from the PPM for export. To answer this question, we fused the exported membrane protein, skeleton binding protein 1 (SBP1), with the rapid, efficient, promiscuous biotin ligase known as TurboID ($SBP1^{TbID}$). Our data show that the $SBP1^{TbID}$ fusion protein was exported efficiently to the host RBC and was able to rapidly biotinylate proteins at the host-parasite interface during its export as well as at its final destination in the host RBC. Using time-resolved, proximity biotinylation and label-free quantitative proteomics, we identified early (pre-export) interactors and late (post-export) interactors of $SBP1^{TbID}$. This led to the identification of 24 proteins that were 10-fold or more enriched in the pre-export time point compared to the post-export time point. Among these early interactors were two promising membrane-associated proteins, one of which has a predicted translocon domain, that could potentially act as translocons at the PPM for exported membrane proteins (Plasmodium translocon of exported membrane proteins or PTEM). Conditional mutants of these candidates suggests that both proteins play essential roles in the asexual lifecycle of the parasite. Both proteins localize to the host-parasite interface during early stages of the intraerythrocytic cycle suggesting that they may play a role in extracting membrane proteins from the PPM for export to the host RBC.

37 # INTRODUCTION

38 Malaria is a major global health issue with an estimated 241 million cases and 627 000
39 deaths reported during 2020[1]. This life-threatening disease is caused by apicomplexan
40 parasites of the genus *Plasmodium*, however one species, *P. falciparum*, is the most
41 virulent and lethal, accounting for 95% of all malaria deaths[2]. The malaria symptoms
42 include headaches, myalgia, high fevers, severe anemia, pulmonary and renal failure,
43 vascular obstruction, and cerebral damage. These disorders could persist even after
44 parasite clearance and are a consequence of parasite proliferation within human red
45 blood cells (RBC)[2,3].

46 To establish infection during their intraerythrocytic cycle, *P. falciparum* parasites must
47 extensively remodel the morphology and physiology of the RBCs. This transformation
48 requires the export of several hundred proteins (about 10% of the parasite proteome)
49 across the unique parasitophorous vacuole (PV) into the RBC cytoplasm and
50 membrane[4–7], and leads to increased permeability, loss of cell deformability, and
51 formation of virulence-associated knobs at the RBC membrane[8,9]. This multi-step
52 transformation is essential for parasite survival and pathogenesis, conferring *P.*
53 *falciparum* its ability to maintain chronic infections in humans. A large fraction of
54 exported proteins are recognizable by the presence of a 5-amino acid motif, known as
55 the *Plasmodium* export element or PEXEL[10,11], while others have no discernable
56 primary sequence motif and are termed as PEXEL-negative exported proteins or
57 PNEPs[12]. Most PNEPs possess a transmembrane (TM) domain that serves to target
58 them to the ER and the secretory pathway[12]. Several of these PNEPs play a critical role
59 in malaria pathogenesis, such as skeleton-binding protein 1 (SBP1)[13–15], membrane
60 associated histidine-rich protein (MAHRP1)[16,17] and erythrocyte membrane protein 1
61 (PfEMP1)[18–20].

62 Exported membrane proteins are inserted into ER membrane during their
63 synthesis[12,21,22]. These membrane proteins are transported via vesicles from the ER
64 and inserted into the parasite plasma membrane (PPM) when the transport vesicles
65 fuse to the PPM[22]. While it has been shown that all exported proteins require the

66 *Plasmodium* translocon of exported proteins, or the PTEX complex to cross the PV
67 membrane (PVM)[23,24], how membrane proteins are extracted from the PPM and
68 delivered to the PTEX complex is unknown. It has been postulated that a putative
69 *Plasmodium* translocon of exported membrane proteins (which we term as PTEM)[25,26] is
70 required for extraction of membrane proteins from the PPM either alone or in
71 cooperation with the PTEX unfoldase HSP101[27,28] (Figure 1A). The identity of proteins
72 in this putative PTEM complex is unknown and there are no obvious candidates in the
73 genome of *P. falciparum*. Therefore, we attempted to utilize an unbiased proteomic
74 approach to identify proteins that could form a putative PTEM complex.

75 Proteomic approaches have been used previously to identify the exported-protein
76 interacting complex (EPIC) at the PV, which is thought to be required for protein
77 export[29]. Similar approaches using *Plasmodium* exported proteins have identified stable
78 complexes at the Maurer's clefts (MC), a parasite-generated protein sorting organelle in
79 the RBC[30,31,32,33]. However, the identification of the putative PTEM has proven elusive
80 because its interaction with exported membrane proteins will be transient and therefore,
81 unlikely to be captured using immunoprecipitation assays which are heavily biased
82 towards identifying stable complexes. Therefore, we used a rapid, proximity-labeling
83 approach to attempt to identify a putative PTEM complex and to our knowledge, this
84 approach has not yet been used in a time-resolved manner to capture transient
85 interactions in the secretory pathway.

86 We chose to tag the endogenous SBP1 gene (PF3D7_0501300) with a new iteration of
87 the promiscuous biotin ligase BirA, known as TurboID (generating $SBP1^{TbID}$)[34]. SBP1 is
88 a PNEP with a single transmembrane domain and is exported in early ring-stage
89 parasites to the MC[13]. TurboID is a highly efficient enzyme that is able to biotinylate
90 proteins in close proximity within 10 minutes[34]. Therefore, we hypothesized that
91 $SBP1^{TbID}$ will biotinylate proteins, even those transiently interacting with $SBP1^{TbID}$ along
92 the secretory pathway during its export to the MC. Since $SBP1^{TbID}$ should rapidly
93 biotinylate proximal proteins, we further reasoned that we could differentiate early (pre-
94 export) interactors from late (post-export) interactors of $SBP1^{TbID}$. Our data show that
95 the $SBP1^{TbID}$ fusion protein is exported to the MC efficiently and with similar kinetics to

96 another MC protein, MAHRP1. Critically, SBP1^{TbID} is able to rapidly biotinylate proximal
97 proteins prior to its export from the PV as well as after export at the MC. Using label-
98 free quantitative proteomics, we compared pre-export interactors and post-export
99 interactors of SBP1^{TbID}. This approach led to the identification of two membrane
100 associated proteins that may be part of the putative PTEM complex.

101 RESULTS

102 SBP1 fused to TurboID is exported to Maurer's Clefts

103 Using CRISPR/Cas9 gene editing we generated mutants of SBP1 (Fig. 1B), where the
104 endogenous gene was tagged with the TurboID biotin ligase (SBP1^{TbID})[34,35]. We chose
105 TurboID because it is an optimized version of the biotin ligase BirA[34]. TurboID is a
106 highly active mutant of BirA with an increased biotinylation radius and faster
107 biotinylation kinetics[34,35]. PCR analysis of genomic DNA isolated from the SBP1^{TbID}
108 parasite line showed the correct integration of the TurboID biotin ligase and a V5 tag at
109 the endogenous locus of SBP1 (Fig. 1C). We detected expression of the SBP1^{TbID} in the
110 mutant line at the expected size, but not in the parental line (Fig. 1D). To ensure that the
111 expression of TurboID is not detrimental to the parasite, we observed the growth of
112 SBP1^{TbID} and the parental parasite line (NF54^{attB})[36], over several asexual cycles using
113 flow cytometry (Fig. 1E). These data show no difference in the asexual growth of
114 SBP1^{TbID} compared to the parental parasites, demonstrating that expression of TurboID
115 or its fusion to SBP1 does not inhibit parasite growth.

116 SBP1 is an exported protein with a single transmembrane domain synthesized in the
117 parasite ER and transported to the MC in the RBC cytoplasm[37,38]. Therefore, we wanted
118 to ensure that the fusion of TurboID to SBP1 did not inhibit its export to the MC. Using
119 immunofluorescence microscopy (IFA), we tested if SBP1^{TbID} colocalized with another
120 MC resident protein, MAHRP1[17]. These data show that SBP1^{TbID} is exported from the
121 parasite to the MC and co-localizes with MAHRP1 during trophozoite and schizont
122 stage parasites (Fig. 1F and 1G). On the other hand, in early ring stage parasites, these
123 data show that SBP1^{TbID}, as well as MAHRP1, localize to the periphery of the parasite,
124 probably in the PV prior to export (Fig. 1F). This has been previously observed by

electron microscopy, where SBP1 accumulated in electron dense regions within the parasite plasma membrane (PPM) before being transported through the PV membrane[39]. These data suggest that SBP1 and possibly other MC resident proteins accumulate in the PV before being exported to the infected RBC. Together, the data show that tagging SBP1 with the TbID biotin ligase did not alter the asexual growth or development of the parasite, nor did it inhibit the export of SBP1 to the host RBC and MC.

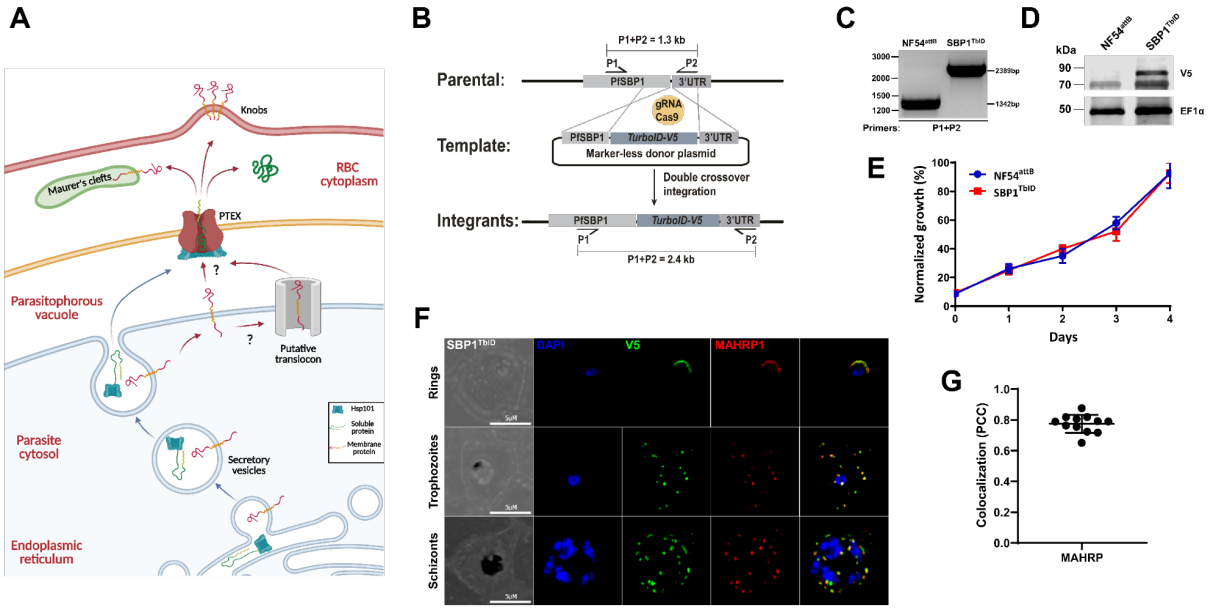

Figure 1. Generation of SBP1^{TbID} mutants. (A) Schematic of protein export. Membrane and soluble proteins are transported from the ER into the PV by secretory vesicles. Soluble proteins are released into the PV lumen after fusion of the secretory vesicle to the PPM. Membrane proteins, on the other hand, are inserted into the PPM and need to be extracted from the membrane by a putative translocon (PTEM) for further transport through the PV membrane to the RBC cytoplasm by the PTEX complex. Soluble and membrane proteins are transported to their final location in the infected RBC. (B) Schematic showing the integration of the repair plasmid used to tag the genomic loci of SBP1 with TurboID-V5. Cas9 introduces a double-stranded break at the C-terminus of the SBP1 locus. The repair plasmid provides homology regions for double-crossover homologous recombination, introducing TurboID and the V5 tag sequences. (C) PCR test confirming integration at the SBP1 locus. Amplicons were amplified from genomic DNA isolated from mutant and wild-type parasites. Primers were designed to amplify the region between the C-terminus and the 3'UTR of SBP1. All primers are in Supplemental Table 1. (D) Western blot of parasite lysates isolated from the parental line (NF54^{attB})[36] and a clone of SBP1^{TbID} (D10) probed with antibodies against V5 and EF1α (loading control). The protein marker sizes are shown on the left. (E) Growth of asynchronous SBP1^{TbID}

149 parasites, compared to the parental line NF54^{attB}, over 4 days via flow cytometry. 100%
150 represent the highest value of calculated parasitemia. Representative of three biological
151 replicates shown for each growth curve. Each data point represents the mean of three technical
152 replicates; error bars represent standard deviation. (F) IFA showing SBP1^{TbID} localizes to the
153 parasite periphery in early-ring stage (top) and is exported to the Maurer's cleft in trophozoite
154 (middle) and schizont (bottom) stages. Asynchronous SBP1^{TbID} parasites were fixed with
155 acetone and stained with specific antibodies. Images from left to right are phase-contrast, DAPI
156 (nucleus, blue), anti-V5 (green), anti-MAHRP (red), and fluorescence merge. Z stack images
157 were deconvolved and projected as a combined single image. (G) Quantification of the
158 colocalization of SBP1^{TbID} with MAHRP using the Pearson's correlation coefficient. Three
159 biological replicates represented with 4 late-stage-parasite images from each replicate. Error
160 bars represent standard deviation.

161

162 Biotin-dependent proximity labeling by SBP1^{TbID}

163 Since our data show that the SBP1^{TbID} fusion protein was exported to MC, we wanted to
164 examine the capacity of TurboID to biotinylate proximal proteins in SBP1^{TbID} parasites.
165 TurboID is an extremely efficient enzyme and we observed it could utilize the minimal
166 amount of biotin present in the media used to grow SBP1^{TbID} parasites (Fig. S1). The
167 normal asexual development of *P. falciparum* does not require biotin[40]. To test if
168 SBP1^{TbID} biotinylation is dependent upon the presence of exogenous biotin, we
169 analyzed protein extracts of asynchronous parasites in the presence or absence of
170 biotin by streptavidin blotting. We observed that efficient biotinylation of proximal
171 proteins occurs only in the presence of biotin in SBP1^{TbID} parasites (Fig. 2A). Self-
172 biotinylation in SBP1^{TbID} parasites was observed in the presence or absence of biotin
173 (Fig. 2A, lane 3 and 4, see asterisk), in agreement with has been previously reported
174 when tagging proteins with TurboID[34,41]. No endogenous biotinylation was detected in
175 the parental line NF54^{attB}, showing that biotinylation occurs only when TurboID is being
176 expressed by the parasite line (Fig. 2A, lane 1 and 2). These data show that SBP1^{TbID}
177 efficiently biotinylates proteins and its activity is dependent upon the presence of biotin
178 in the growth medium.

179 TurboID is a highly active enzyme[34] that offers the possibility of rapid and time-resolved
180 labeling approaches in contrast to previous proximity-labeling methods with much
181 longer incubation times, usually greater than 12 hours[42–44]. Thus, we wanted to assess

182 the biotinylation activity SBP1^{TbID} and test whether this fusion protein is able to rapidly
183 biotinylate proximal proteins. SBP1^{TbID} parasites were incubated with biotin for 1, 2 or 6
184 hours and the biotinylation of proteins were observed using western blots probed with
185 streptavidin (Fig. 2B). We also tested biotinylation in response to different
186 concentrations of biotin, 25, 50 and 100 μM (Fig. 2C). Biotinylated proteins were
187 observed at all time points and biotin concentration, and the observable difference in the
188 extent of protein biotinylation between the time points and concentrations was minimal
189 (Fig. 2B and 2C).

190 The SBP1^{TbID} fusion protein has to traverse several membranes during its export to the
191 MC, and therefore, it is likely to unfold and then refold during this transport process. In
192 the case of exported membrane proteins, it is not known if they are kept unfolded during
193 their transport, though all proteins have to unfold while crossing the PV membrane
194 using the PTEX complex at the PV membrane[23,24,45]. Furthermore, to our knowledge
195 TurboID has not yet been utilized in a time-resolved manner to identify transient
196 interactors as proteins are transported through the secretory pathway. Therefore, we
197 wanted to determine if SBP1^{TbID} parasites could biotinylate proteins proximal to SBP1 at
198 different cellular locations during the export of SBP1^{TbID} from the parasite ER to the MC.
199 Synchronized early ring and trophozoite stage parasites were observed by IFAs after
200 the addition of biotin for 2 h. We observed biotinylation at the parasite periphery,
201 possibly when SBP1^{TbID} accumulates at the PV[39] (Fig. 2D, top panels). Biotinylation was
202 also observed when SBP1^{TbID} had been exported to the MC (Fig. 2D, bottom panels).
203 The observed biotinylation was dependent upon the addition of biotin. Together, these
204 data demonstrate that SBP1^{TbID} was highly active, efficient, rapid, and labeled proximal
205 proteins at different subcellular locations during its export from the parasite ER to the
206 final location at the MC.

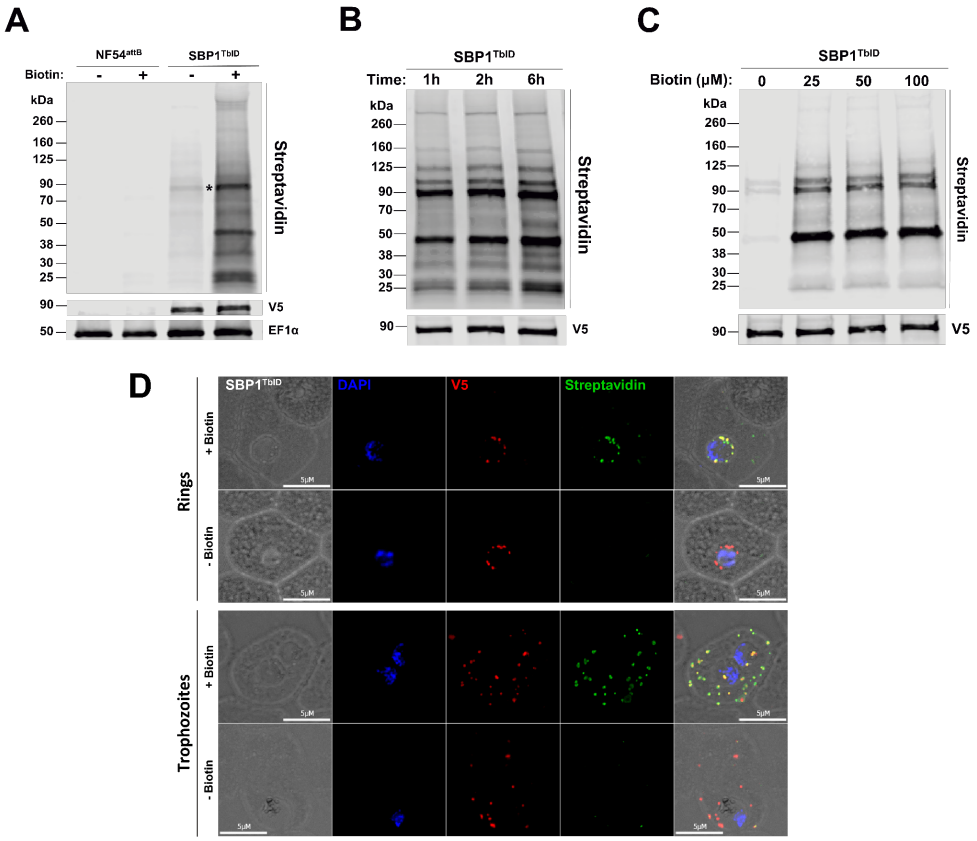

Figure 2. Biotinylation of proximal proteins by TurboID$_{V5}$-tagged SBP1. (A) Western blot of parasite lysates isolated from the parental line NF54^{attB} and the mutant line SBP1^{TbID} incubated with or without biotin (50 μM) for 2 h. Samples were probed with antibodies against V5, EF1α (loading control) and fluorescent dye-labeled streptavidin. The protein marker sizes are shown on the left. (B) Western blot of parasite lysates isolated from the mutant line SBP1^{TbID} incubated with biotin (50 μM) for 1 h, 2h and 6h. Samples were probed with antibodies against V5 (loading control) and fluorescent dye-labeled streptavidin. The protein marker sizes are shown on the left. (C) Western blot of parasite lysates isolated from the mutant line SBP1^{TbID} incubated with different concentrations of biotin (0, 25, 50 and 100 μM) for 1 h. Samples were probed with antibodies against V5 (loading control) and fluorescent dye-labeled streptavidin. The protein marker sizes are shown on the left. (D) IFA showing SBP1^{TbID} biotinylates proteins during their export out of the parasite (top panels) and at their final location at the Maurer's clefts (Bottom panels). Asynchronous SBP1^{TbID} parasites were fixed with acetone after 2 h of incubation with biotin (50 μM) and stained with specific antibodies. Images from left to right are phase-contrast, DAPI (nucleus, blue), anti-V5 (red), streptavidin (green), and fluorescence merge. Z stack images were deconvolved and projected as a combined single image.

225 ## Early interactors of SBP1^{TbID} identified by proximity labeling

226 Since our data show that SBP1^{TbID} biotinylates proximal proteins during its transport
227 from the parasite ER into the RBC cytoplasm (Fig. 2C), we next wanted to identify the
228 *P. falciparum* effectors that interact with SBP1 at the host-parasite interface. To do so,
229 we wanted to define the kinetics of SBP1^{TbID} transport from its site of synthesis in the
230 parasite ER to the MC and test if we could reproducibly detect SBP1 at the host-
231 parasite interface. As previously described (Fig. 1E, 2C), SBP1^{TbID} and proteins
232 biotinylated by SBP1^{TbID} could be detected at the parasite-RBC interface. To assess
233 whether we could reproducibly observe SBP1^{TbID} within the parasite prior to its export to
234 the host RBC, we used tightly synchronized cultures and observed the subcellular
235 localization of SBP1^{TbID} with respect to EXP2, a PVM resident protein[46,47], at different
236 time points after parasite invasion. SBP1 has been detected at the MCs as early as 4-6
237 hours post invasion (hpi)[48], therefore, we observed the subcellular location of SBP1^{TbID}
238 in parasites at 3, 4 and 5 hpi. In some SBP1^{TbID} parasites, SBP1 was either not
239 detectable or not expressed (Fig. 3B, top panels). As expected, we found parasites
240 where SBP1^{TbID} was within the PV periphery, and others where the protein was already
241 exported to the RBC cytoplasm (Fig. 3C, mid and bottom panels). We quantified these
242 three events over several biological replicates. At 4hpi, SBP1^{TbID} was not expressed in
243 about 30% of the parasites, exported in ~10% of observed parasites and at the host-
244 parasite interface in the vast majority (60%) of all parasites (Fig. 3C). These data
245 showed us that harvesting proteins biotinylated by SBP1^{TbID} at the host-parasite
246 interface was feasible.

247 To identify early interactors of SBP1, especially those at the host-parasite interface, we
248 opted for a quantitative and comparative approach. We wanted to differentiate these
249 early interactors from SBP1 interactors at the MC, which have been previously
250 identified[32], as well as those being co-transported with SBP1 to the MC. We
251 hypothesized that using label-free quantitative proteomics and comparing interactors
252 isolated from 4 hpi and 20 hpi would allow us to identify the early interactors of SBP1.
253 By 20 hpi, all SBP1 is at the MCs and no more SBP1 is synthesized[49]. Label-free
254 proteomics have been shown to offer a large dynamic range and high proteome

255 coverage in the identification of biotinylated proteins[41,50–52].

256 First, tightly synchronized late-stage schizonts were collected. These parasites were
257 then split into two samples, one incubated with biotin for 4 h until 4 hpi (Fig. 3A, blue
258 square) and then collected for further processing. Since our data show that in the
259 majority of the 4 h ring stage parasites, SBP1^{TbID} was at the host-parasite interface (Fig.
260 3C), parasites were incubated with biotin for 4 h to maximize the labeling of proximal
261 proteins and capture a larger fraction of the pre-export interactors. To collect the post-
262 export sample, we let SBP1^{TbID} parasites develop until 16hpi because all SBP1 localizes
263 to MC by this time and this protein is no longer synthesized. Thus, the other sample was
264 allowed to develop without biotin for 16h, and then incubated with biotin for 4 h until 20
265 hpi (Fig. 3A, red square). Biotinylated proteins were isolated from parasite lysates using
266 streptavidin-affinity pulldown. Streptavidin-captured proteins were identified via mass
267 spectrometry (MS) and quantified over several biological replicates[41,50,51] (Fig. 4A). A
268 total of 1,122 proteins were identified in at least one of the replicates. We then
269 compared the proteins identified in the 4h sample with those identified in the 20h
270 sample (Fig. 4B). We defined the putative pre-export interactors of SBP1 from our
271 dataset using three stringent criteria. Proteins enriched more than 10-fold compared to
272 the 20 hpi samples with a p-value cut-off of 0.05, and present in all three biological
273 replicates were considered as differentially labeled interactors at 4 hpi. Using these
274 criteria, 24 protein candidates were identified as putative pre-export interactors of
275 SBP1^{TbID} during its transport at the parasite-RBC interface (Figure 4B). The identified
276 proteins were classified into subgroups based on their predicted functions and
277 subcellular locations[53]. Of the 24 identified proteins, 11 were uncharacterized proteins
278 with no predicted function. As expected, this approach identified proteins known to be
279 involved in protein and vesicle transport (5/24). One of the statistically significant
280 interactors of SBP1 was EXP3 (3-fold enriched at 4hpi), which has been localized to the
281 PV and functions in protein export [29]. The experiment worked as designed because
282 SBP1 (star, Figure 4B) and other MC localized as well exported proteins were also
283 identified but were not enriched at either time point or enriched at the 20hpi samples
284 (Figure 4B). Identification of exported proteins, including MC proteins, only in the post-

285 export (20hpi) samples further suggests that the proteomic approach using SBP1^{TbID}
286 worked as designed. Together these data showed that our approach successfully
287 identified a group of proteins differentially biotinylated by SBP1^{TbID} prior to its export to
288 the MC.

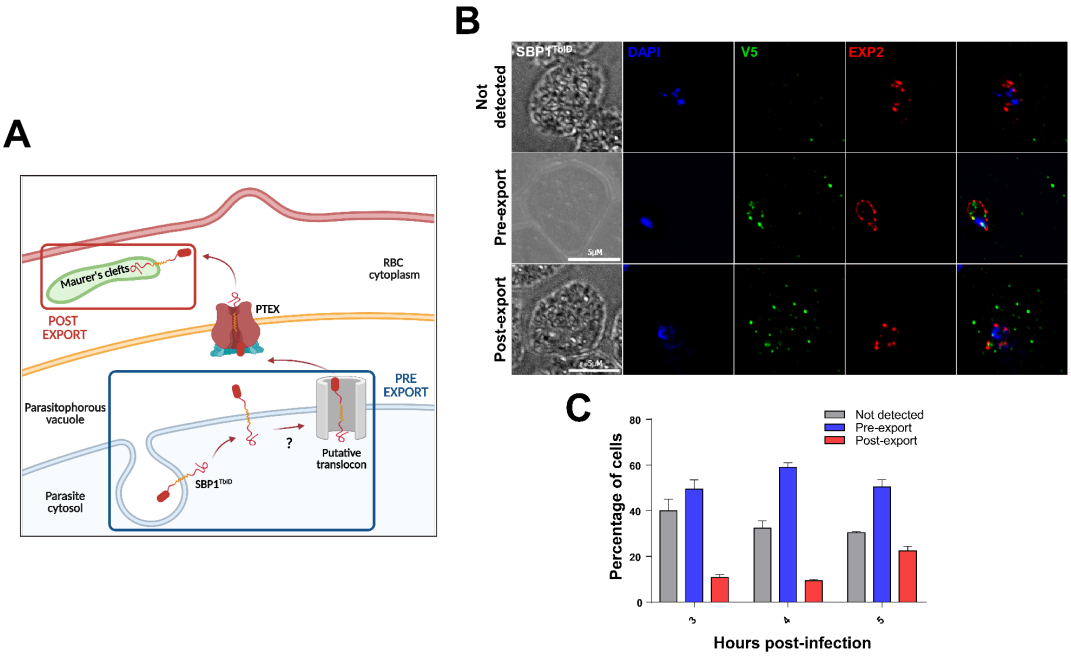

289

290 **Figure 3.** (A) Schematic of the export of proteins in *P. falciparum* highligting the locations where
291 proteins biotinylated by SBP1^{TbID} will be harvested. Created with BioRender.com. (B) IFA
292 showing the different localizations of SBP1^{TbID} during its export at early ring-stages (3-5 hpi).
293 Tightly synchronous SBP1^{TbID} parasites were fixed with acetone at 3 h, 4h and 5 h post
294 infection, and stained with specific antibodies. Images from left to right are phase-contrast, DAPI
295 (nucleus, blue), anti-V5 (green), EXP2 (PV marker, green), and fluorescence merge. Z stack
296 images were deconvolved and projected as a combined single image. (C) Quantification of the
297 events observed in (B). Events were scored based on the localization of SBP1^{TbID} with respect
298 to the PV marker EXP2. A total of 50 parasites were scored for each time point. n= 3 biological
299 replicates; error bars represent standard deviation.

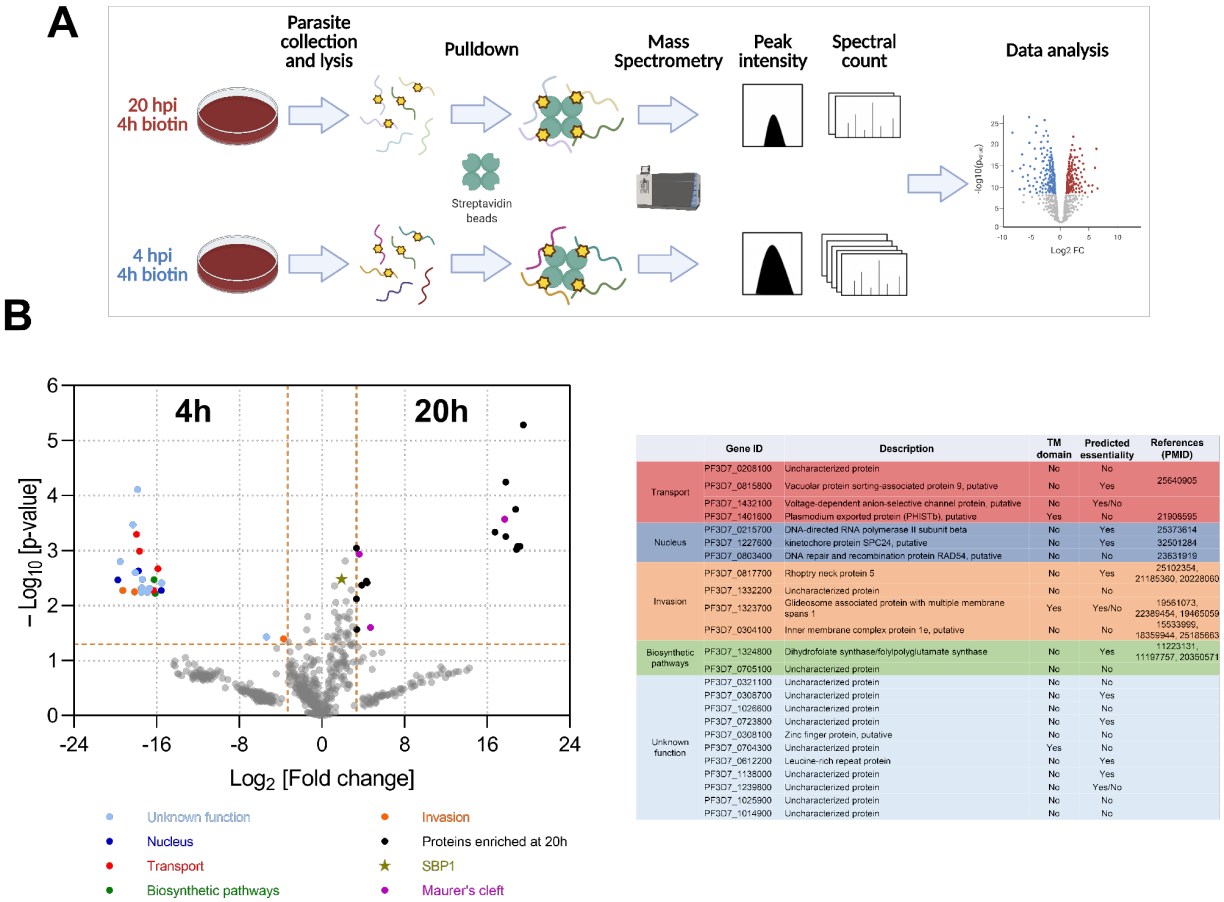

	Gene ID	Description	TM domain	Predicted essentiality	References (PMID)
Transport	PF3D7_0208100	Uncharacterized protein	No	No	25640905
	PF3D7_0815800	Vacuolar protein sorting-associated protein 9, putative	No	Yes	
	PF3D7_1432100	Voltage-dependent anion-selective channel protein, putative	No	Yes/No	
	PF3D7_1401600	Plasmodium exported protein (PHISTb), putative	Yes	No	21906595
Nucleus	PF3D7_0215700	DNA-directed RNA polymerase II subunit beta	No	Yes	25373614
	PF3D7_1227600	kinetochore protein SPC24, putative	No	Yes	32501284
	PF3D7_0803400	DNA repair and recombination protein RAD54, putative	No	No	23631919
Invasion	PF3D7_0817700	Rhoptry neck protein 5	No	Yes	25102354, 21185360, 20228060
	PF3D7_1332200	Uncharacterized protein	No	No	
	PF3D7_1323700	Gliideosome associated protein with multiple membrane spans 1	Yes	Yes/No	19561073, 22389454, 19465059
	PF3D7_0304100	Inner membrane complex protein 1e, putative	No	No	15533999, 18359944, 25185683
Biosynthetic pathways	PF3D7_1324800	Dihydrofolate synthase/folylpolyglutamate synthase	No	Yes	11223131, 11197757, 20350571
	PF3D7_0705100	Uncharacterized protein	No	No	
Unknown function	PF3D7_0321100	Uncharacterized protein	No	No	
	PF3D7_0308700	Uncharacterized protein	No	Yes	
	PF3D7_1026600	Uncharacterized protein	No	No	
	PF3D7_0723800	Uncharacterized protein	No	Yes	
	PF3D7_0308100	Zinc finger protein, putative	No	No	
	PF3D7_0704300	Uncharacterized protein	Yes	No	
	PF3D7_0812200	Leucine-rich repeat protein	No	Yes	
	PF3D7_1138000	Uncharacterized protein	No	Yes	
	PF3D7_1239800	Uncharacterized protein	No	Yes/No	
	PF3D7_1025900	Uncharacterized protein	No	No	
	PF3D7_1014900	Uncharacterized protein	No	No	

Figure 4. (A) Schematic of the experimental design for time-resolved biotinylation and proteomics to identify pre-export and post-export interactors of SBP1^{TbID}**.** Created with BioRender.com. (B) Interactors enriched at 4 hpi (p-value plotted as function of fold change between the two samples). Proteins with p-value ≤0.05 and more than 10-fold change are identified as SBP1^{TbID} interactors. n= 3 biological replicates. (C) A summary table of the putative interactors of SBP1^{TbID} at 4hpi grouped by their putative functions are shown. All proteins identified are in Supplemental Table 2.

Early interactors of SBP1^{TbID} localize to the host-parasite interface

Since we were interested in identifying proteins that may act as a putative translocon to extract exported membrane proteins at the PPM, we reasoned that membrane associated proteins among pre-export SBP1 interactors could function in this role. Thus, based on membrane-association, high statistical score and fold enrichment, we selected

314 the Glideosome-associated protein with multiple membrane spans 1 (GAPM1,
315 PF3D7_1323700) as one putative candidate. GAPM1 is a membrane protein associated
316 with the biogenesis of the Inner Membrane Complex (IMC) in asexual and sexual
317 stages. GAPM1, as part of the IMC, is suggested to have a role in merozoite invasion[54–
318 56]. Using these criteria, another putative candidate was the channel protein Voltage-
319 dependent anion-selective channel protein (VAC, PF3D7_1432100). VAC is a soluble
320 protein with a translocon of outer mitochondrial membrane (TOM40) domain but no
321 mitochondria targeting signal. Nothing is known about the function of VAC in *P.*
322 *falciparum*.

323 To characterize these proteins we used CRISPR/Cas9 gene editing to generate the
324 conditional mutants, termed VAC^{apt} and GAPM1$^{mNG\text{-}apt}$. In these parasite lines, their
325 endogenous loci were tagged with the *tetR* aptamer system, which results in
326 anhydrotetracycline (aTc)-dependent expression of protein (Fig. 5A and 5B)[57]. PCR
327 analysis of genomic DNA from VAC^{apt} and GAPM1$^{mNG\text{-}apt}$ parasite lines showed correct
328 integration of the knockdown system at the endogenous loci (Fig. S5A). To assess the
329 efficiency of the knockdown system, we measured protein expression in the presence or
330 absence of aTc by Western blotting. For both proteins, there is a clear reduction of
331 protein expression (Fig. S5B), which in the case of GAPM1$^{mNG\text{-}apt}$ was detrimental, as
332 parasites were not able to progress into a second life cycle. Knockdown of VAC
333 inhibited the asexual expansion of VAC^{apt} parasites (Fig. S5C).

334 Our data show that GAPM1^{mNG} localizes to the IMC in schizonts (Fig. S3). However,
335 what happens to the IMC after merozoite invasion is unclear and we reasoned that the
336 IMC most likely fuses to the PPM shortly after invasion. Similarly, the subcellular
337 localization of VAC during the early stages of the asexual lifecycle was unknown. The
338 proteomic data suggest that these proteins are in close proximity to SBP1^{TbID} when
339 SBP1 is in the PV (Fig. 4B). Therefore, we used IFAs to localize both proteins in tightly
340 synchronized parasites at 4 hpi with respect to the PV marker EXP2. VAC^{apt} localizes to
341 the parasite periphery and is closely juxtaposed with the known PV marker, EXP2, but it
342 also partially overlaps with the mitochondria (Fig. 5C, top panels) suggesting that it may
343 be localized to both subcellular organelles. GAPM1$^{mNG\text{-}apt}$ localizes to the parasite

344 periphery at 4 hpi, and shows colocalization with EXP2 (Fig. 5C, bottom panels). To
345 corroborate our observations by IFAs, we used structured illumination microscopy (SIM)
346 to determine the subcellular localization of VAC and GAPM1. Both proteins show a
347 juxtaposed localization with respect to the PVM marker EXP2, which suggests VAC and
348 GAPM1 do not localize to the PVM but rather to a different membrane such as the PPM
349 (Fig. 5D). Together these results show that both GAPM1 and VAC localize to the same
350 region together with SBP1^{TbID} at the PV at 4 hpi, as suggested by the proximity labeling
351 data.

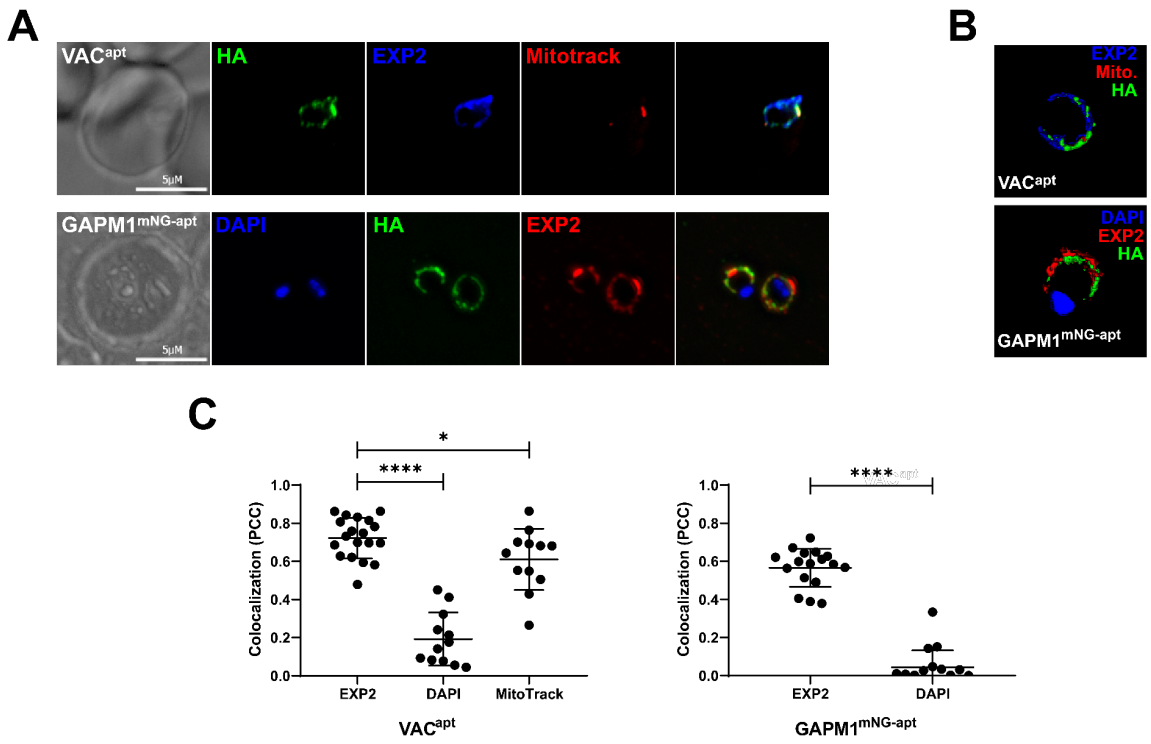

352

353 **Figure 5. Generation and characterization of VAC^{apt} and GAPM1$^{mNG-apt}$.** (A) Representative
354 IFA showing VAC^{apt} and GAPM1$^{mNG-apt}$ localizes within the PV in the early-ring stage (4 hpi).
355 Tightly synchronous parasites were fixed with PFA (VAC^{apt}) and acetone (GAPM1$^{mNG-apt}$) and
356 stained with specific antibodies. Images of VAC^{apt} from left to right are phase-contrast, anti-HA
357 (green), anti-EXP2 (PV, blue), mitotracker (mitochondria, red), and fluorescence merge. Images
358 of GAPM1$^{mNG-apt}$ from left to right are phase-contrast, DAPI (nucleus, blue), anti-HA (green),
359 anti-EXP2 (PV, red), and fluorescence merge. Z stack images were deconvolved and projected
360 as a combined single image. (B) 3D reconstruction based on structured illumination microscopy
361 images captured from VAC^{apt} and GAPM1$^{mNG-apt}$ ring-stage parasites at 4 hpi and stained with
362 the antibodies as in (A). (C) Quantification of the colocalization of VAC and GAPM1^{mNG} with
363 respect to EXP2, MitoTracker (Mitochondrial marker) and DAPI, and to EXP2 and DAPI,
364 respectively, using the Pearson's correlation coefficient. Three biological replicates represented

365 with 6 parasite images from each replicate for EXP2, and 3 parasite images for MitoTrack and
366 DAPI. Error bars represent standard deviation. ****p<0.05 by t-student test.

367

368 # DISCUSSION

369

370 The protein-protein interactions that usher exported proteins to their final destinations in
371 the RBC via the secretory pathway are transient in nature. Previously, IP-based methods
372 have been used to identify proteins required for export of *P. falciparum* proteins, such as
373 the PTEX complex[58] and the EPIC complex[29]. While IP-based approaches are well-suited
374 for identifying stable complexes, they are unlikely to identify transient interactions. A
375 putative additional translocon at the PPM required for extracting exported membrane
376 proteins which are inserted into the PPM during transport has long been proposed[25,26].
377 As yet, no candidates for this putative PTEM complex have been identified (Fig. 1).

378

379 In our study, we used time-resolved biotinylation to identify transient interactions of an
380 exported membrane protein, SBP1, during its export. This approach uses a rapid and
381 promiscuous biotin ligase to biotinylate proximal proteins[34]. Since biotinylation is a
382 permanent modification, even transient interactions can be potentially identified. Through
383 this approach, we found putative candidates for a translocon complex that could help
384 extract membrane exported proteins from the PPM for transport into the RBC. Our data
385 show that fusion of TurboID to the exported transmembrane-containing protein, SBP1,
386 did not alter its trafficking to the MC nor did it have any effect on parasite growth. These
387 data also suggest that TurboID is enzymatically active during transit in the parasite
388 secretory pathway.

389 A previous study on the SBP1 interactome at their final location at the Maurer's cleft
390 identified 88 parasite proteins as putative interactors[32]. Most of their top-ranked hit
391 proteins were also identified in our study such as PfEMP1, Pf332, PIESP2, REX1,
392 MAHRP1, PTP1 and vapA. However, these were not highly enriched (≤10-fold) in the
393 post-export interactors fraction. This could be because some of these proteins are co-

394 transported with SBP1 and thus, are identified in the pre-export fraction as well. Members
395 of the PTEX complex such as EXP2, HSP101, and Trx2, were also identified in the pre-
396 export fraction, albeit below statistical significance. In addition, PTP2 and PfG174, that
397 have been previously shown to localize as residents[59], or transient interactors[60] of the
398 Maurer's clefts, were more than 10-fold enriched at the post-export time point,
399 demonstrating the reliability of our approach to identify SBP1 interactors. Another subset
400 of proteins identified in our study as post export interactors of SBP1 are ribosomal
401 proteins, which have been previously observed to be exported to the red blood cell
402 cytoplasm in *P. falciparum*[61]. Together, these data strongly suggest that the time-
403 resolved, rapid biotinylation approach was working as designed. Since our focus was to
404 identify pre-export interactors, we did not pursue these proteins for further study.

405 Using label-free quantitative proteomics, we identified a group of 24 putative candidates
406 that interact with SBP1 prior to its export to the RBC. Several of the proteins identified
407 (14/24) were uncharacterized proteins or nuclear proteins. Since we undertook this
408 approach to identify the proposed translocon of exported membrane proteins, we did not
409 pursue the function of these proteins in this study. Translocons function to transport
410 proteins across membranes and therefore, we hypothesized that membrane associated
411 proteins in this list could putatively function as translocons. There were two putative
412 candidates in the pre-export interactors of SBP1 that were membrane associated, VAC
413 and GAPM1. However, their localization in early ring stage parasites was unknown.
414 Therefore, to study the function of VAC and GAPM1 in early ring stage parasites, we
415 successfully generated conditional mutants. The data show that both VAC and GAPM1
416 play important functions in parasite survival within the infected RBC. Knockdown of these
417 proteins inhibits parasite growth. However, achieving protein knockdown takes about 24-
418 48 hours and results in parasite death prior to invasion of the RBC. Therefore, this
419 prevents the characterization of their role in export, which occurs in about 6-8 hours after
420 invasion. Similar to the PTEX translocon, EXP2[46], it is likely that both GAPM1 and VAC
421 have other essential functions in the asexual lifecycle. Defining their function in export will
422 require using a more rapid knockdown approach with similar kinetics as SBP1 export,
423 such as degradation-domain based tools[23,62] or rapid mislocalization based methods[63].

424

425 VAC has a β-barrel porin domain that can form an aqueous channel in the membrane and
426 function as a translocon in mitochondria and other plastids[64]. In a recent proximity-
427 biotinylation based proteomic screen to catalog mitochondrial proteins in *P. falciparum*,
428 VAC was pulled down in the membrane fraction of parasite lysates, and not in the
429 mitochondrial fraction[65]. In addition, VAC is predicted to not contain a mitochondrial
430 targeting sequence, in contrast to its Plasmodium ortholog, TOM40 (PF3D7_0617000),
431 which has a mitochondrial targeting sequence, suggesting that VAC it might not be
432 localized to the mitochondria[66]. Our data reveal that VAC localizes at the host-parasite
433 interface in early ring stages. While there is some overlap of VAC with the mitochondria,
434 there is stronger overlap between the PVM marker, EXP2, and VAC in lower resolution
435 IFAs. It is also possible that VAC is dually localized both to the mitochondria as well as to
436 the host-parasite interface. Superresolution microscopy suggests that EXP2 and VAC are
437 closely juxtaposed but with minimal overlap. This suggests that VAC localizes to a
438 compartment in close proximity to the PVM, most likely the PPM. On the other hand,
439 GAPM1 has seven TM domains and is from an apicomplexan-specific family of proteins[56].
440 GAPM1 has been localized to the inner membrane complex (IMC) in schizont-stage
441 parasites[56]. The IMC plays an essential role in the invasion of merozoites into the RBC,
442 however, it is unclear what happens to the IMC post-invasion. Lower resolution IFAs show
443 that GAPM1 co-localizes with the PVM localized EXP2 in early ring stage parasites. In
444 superresolution microscopy we observe, similar to VAC, GAPM1 in close juxtaposition
445 with EXP2, but does not completely overlap, suggesting that GAPM1 may also localize to
446 the PPM in early rings. These data further suggest that the IMC may fuse to the parasite
447 plasma membrane after merozoite invasion. Together, these findings suggest that VAC
448 and GAPM1 transiently interact with SBP1 prior to its export and their localization to the
449 parasite periphery suggests a role in export, perhaps as members of a putative PTEM
450 complex. Based on these data, we propose a model where GAPM1 and VAC act together
451 to select and extract exported proteins from the PPM for further transport via the PTEX
452 into the host RBC.
453

454 Several mechanistic aspects of this model remain to be resolved but similar to the PTEX
455 complex, which was first identified as a putative complex at the PV membrane[58], both
456 VAC and GAPM1 are at the right place at the right time. Further, VAC has a porin
457 translocon domain which could function in a manner analogous to the mitochondrial outer
458 membrane translocon to extract membrane anchored exported proteins from the parasite
459 plasma membrane. This hints that this ancient porin domain protein has been repurposed
460 by *Plasmodium* parasites on the PPM to facilitate export of membrane proteins to the
461 infected RBC.

462

463 # ACKNOWLEDGEMENTS

464 We thank Dan Goldberg for anti-EF1α; Hans-Peter Beck for anti-MAHRP1; the
465 European Malaria Reagent Repository for anti-EXP2; Julie Nelson at the CTEGD
466 Cytometry Shared Resource Laboratory for help with flow cytometry and analysis; and
467 Muthugapatti Kandasamy at the Biomedical Microscopy Core at the University of
468 Georgia for help with microscopy. We acknowledge the assistance of Phil Gafken at the
469 Proteomics Resource at Fred Hutchinson Cancer Research Center for mass
470 spectrometry and data analysis. The study was funded by NIH/NIAID R01AI130139
471 (V.M.), T32AI060546 (D.W.C.), and Office of the Vice-President for Research at UGA
472 (D.A.).

473

474

475 # MATERIALS AND METHODS

476 ## Construction of SBP1 plasmids

477 Genomic DNA was isolated from *P. falciparum* NF54^{attB} cultures using the QIAamp DNA
478 blood kit (Qiagen). PCR products were inserted into the respective plasmids using
479 ligation-independent cloning (SLIC), as described earlier [67], or the NEBuilder HiFi DNA

480 Assembly system (NEB). All constructs used in this study were confirmed by
481 sequencing. All primers used in this study are in Supplemental Table 1.

482 For generation of the plasmid pTOPO-SBP1-TbID, sequences of approximately 500 bp
483 of homology to the SBP1 C-terminus and 3'UTR were amplified using primer pairs P1-
484 P2 and P3-P4, respectively, and the sequence of V5-tagged TurboID was amplified
485 using primers P5 and P6. For expression of a SBP1 gRNA, oligos P17-P18 were
486 inserted into cut pUF1-Cas9.

487 For generation of the plasmid pKD-VAC-Apt, sequences of approximately 450 bp of
488 homology to the Pf1432100 C-terminus and 3'UTR were amplified using primer pairs
489 P7-P8 and P9-P10, respectively. Amplicons were then inserted into pKD[57,67] digested
490 with AatII and AscI. For expression of a Pf1432100 gRNA, oligo P19 was inserted into
491 cut PUF1-Cas9.

492 For generation of the plasmid pKD-GAPM1-mNG-Apt, sequences of approximately 500
493 bp of homology to the PfGAPM1 C-terminus and 3'UTR were amplified using primer
494 pairs P11-P12 and P13-P14, respectively, and the sequence of mNeonGreen was
495 amplified using primers P15 and P16. Amplicons were then inserted into pKD[57] digested
496 with AatII and AscI. For expression of PfGAPM1 gRNA, oligo p20 was inserted into cut
497 PUF1-Cas9.

498 Parasite culture and transfections

499 *Plasmodium* parasites were cultured in RPMI 1640 medium (NF54^{attB}, VAC^{apt} and
500 GAPM1$^{mNG\text{-}apt}$) or in biotin-free medium (SBP1^{TbID}, VAC^{apt}/SBP1^{TbID}) [68] supplemented
501 with AlbuMAX I (Gibco), and transfected as described earlier[69].

502 For generation of SBP1^{TbID} parasites, a mix of two plasmids (50 µg each) were
503 transfected into NF54^{attB} parasites in duplicate. The plasmid mix contained the plasmid
504 pUF1-Cas9-SBP1gRNA, which contains the DHOD resistance gene, and the marker-
505 free plasmid pTOPO-SBP1-TbID. Drug pressure was applied 48 h after transfection,
506 using 1µM DSM1 [70] and selecting for Cas9 expression. After parasites grew back from

507 transfection, integration was confirmed by PCR, and then cloned using limiting dilution.
508 After clonal selection, cultures were transferred to biotin-free medium without DSM1.

509 For generation of VAC^{apt} and GAPM1$^{mNG\text{-}apt}$ parasites, the pKD-VAC-Apt and pKD-
510 GAPM1-mNG-Apt plasmids (20 µg) and the respective pUF1-Cas9 plasmid (50 µg)
511 were transfected into NF54^{attB} parasites in duplicate. Before transfection pKD plasmids
512 were digested overnight with EcoRV (NEB). The enzyme was then subjected to heat
513 inactivation for 20 min at 65 °C and then mixed with the pUF1-Cas9 plasmid.
514 Transfected parasites were grown in 0.5 µM anhydrous tetracycline (aTc) (Cayman
515 Chemical). Drug pressure was applied 48 h after transfection, using blasticidin (BSD) at
516 a concentration of 2.5 µg/mL, selecting for pKD-VAC-Apt and pKD-GAPM1-mNG-Apt
517 expression. After parasites grew back from transfection, integration was confirmed by
518 PCR, and then cloned using limiting dilution. Clones were maintained in mediums
519 containing 0.5 µM aTc and 2.5 µg/mL BSD.

520 For generation of VAC^{apt}/SBP1^{TbID} parasites, a mix of two plasmids: pTOPO-SBP1-TbID
521 and pUF1-Cas9-SBP1gRNA, was transfected into VAC^{apt} parasites. Drug pressure was
522 applied 48 h after transfection, using 1µM DSM1 [70] and selecting for Cas9 expression.
523 After parasites grew back from transfection, integration was confirmed by PCR, and
524 then cloned using limiting dilution.

525 Growth assays

526 For all assays, aliquots of parasite cultures were incubated in 8 µM Hoechst 33342
527 (ThermoFisher Scientific) for 20 min at room temperature and then fluorescence was
528 measured using a CytoFlex S (Beckman Coulter) flow-cytometer. Flow cytometry data
529 were analyzed using FlowJo software (Tree Star, Inc.) and plotted using Prism
530 (GraphPad Software, Inc.).

531 For the SBP1^{TbID} growth assay, asynchronous parasites were transferred to a 96-well
532 plate at 0.5% parasitemia and grown for 4 days. Parasitemia was monitored every 24 h.

533 For the VAC^{apt} and GAPM1$^{mNG\text{-}apt}$ growth assays, synchronous ring-stage parasites
534 were washed 5 times with RPMI 1640 medium and split into two cultures, one
535 resuspended in medium containing 0.5 µM aTc and 2.5 µg/mL BSD, and the other one
536 in medium containing only 2.5 µg/mL BSD. Then cultures were transferred to a 96-well
537 plate at 0.2% parasitemia and grown for 6 days. Parasitemia was monitored every 48 h.

538 Western blotting

539 For SBP1^{TbID} parasites, RIPA buffer (150 mM NaCl, 20mM Tris-HCl pH 7.5, 1mM
540 EDTA, 1% SDS, 0.1% Triton X-100) and sonication were used to disrupt parasite pellets
541 conserving all exported proteins. Briefly, late-stage parasites were isolated using a
542 Percoll gradient (Genesee Scientific). Pellets were then resuspended in RIPA buffer and
543 sonicated 3 times at 20% amplitude for 20 s. Protein supernatants were subsequently
544 solubilized in protein loading dye with Beta-mercaptoethanol (LI-COR Biosciences) and
545 used for SDS-PAGE.

546 For VAC^{apt} and GAPM1$^{mNG\text{-}apt}$ parasites, ice-cold 0.04% saponin in 1x PBS was used to
547 isolate parasites from host cells. Parasite pellets were subsequently solubilized in
548 protein loading dye with Beta-mercaptoethanol (LI-COR Biosciences) and used for
549 SDS-PAGE.

550 Primary antibodies used in this study were mouse-anti-V5 (Cell Signaling Technology,
551 1:1000), rabbit-anti-PfEF1α (from D. Goldberg, 1:2000), and mouse-anti-HA 6E2 (Cell
552 Signaling Technology, 1:2000). Secondary antibodies used were IRDye 680 CW goat-
553 anti-rabbit IgG, IRDye 800CW goat-anti-mouse IgG, and IRDye 800CW Streptavidin (Li-
554 COR Biosciences, 1:20 000 and 1:10 000). Membranes were imaged using the
555 Odyssey Clx Li-COR infrared imaging system (Li-COR Biosciences). Images were
556 processed and analyzed using ImageStudio (Li-COR Biosciences).

557 Immunofluorescence microscopy

558 For IFAs, cells were fixed as described previously [67]. The cell lines SBP1^{TbID} and
559 GAPM1^{apt} were smeared on a slide and fixed with acetone. The cell lines VAC^{apt} and

560 VAC^{apt}/SBP1^{TbID} were fixed with 4% paraformaldehyde (Electron Microscopy Sciences)
561 and 0.03% glutaraldehyde. Primary antibodies used were mouse-anti-V5 TCM5
562 (eBioscience, 1:100), rabbit-anti-V5 D3H8Q (Cell Signaling technology, 1:100), rabbit-
563 anti-HA 71550 (ThermoFisher Scientific, 1:100), rabbit-anti-MAHRP (from H. Beck,
564 1:500), mouse-anti-EXP2 7.7 and mouse-anti-KAHRP (from D. Cavanagh; 1:1000,
565 1:500 respectively). Secondary antibodies used were Alexa Fluor 488, Alexa Fluor 546,
566 and Streptavidin Alexa Fluor 488 (Life Technologies, 1:1000). Cells were mounted using
567 ProLong Diamond with 4',6'-diamidino-2-phenylindole (DAPI) (Invitrogen) and imaged
568 using a DeltaVision II microscope system with an Olympus Ix-71 inverted microscope.
569 Images were collected as a Z-stack and deconvolved using SoftWorx, then displayed as
570 a maximum intensity projection. Adjustments to brightness and contrast were made for
571 display purposes using Adobe Photoshop.

572 Synchronization assays

573 For detection of SBP1 during export, SBP1^{TbID} parasites were synchronized with two
574 series of 5% sorbitol treatment. Then, schizont-stage parasites were isolated using
575 Percoll gradient (Genesee Scientific) and immediately transferred to previously warmed
576 fresh red blood cells at 1% hematocrit. Parasites were allowed to egress and invade
577 new red blood cells, and samples were obtained for IFAs at different time points.

578 SBP1^{TbID} proximity biotinylation and mass spectrometry

579 Biotinylation by TbID-tagged SBP1 was confirmed by collecting SBP1^{TbID} parasites for
580 Western blotting and IFAs after incubation for 2 h in biotin-free media supplemented
581 with 50 μM biotin.

582 For detection of SBP1 during export, SBP1^{TbID} parasites were synchronized with two
583 series of 5% sorbitol treatment. Then, late-schizont-stage parasites were isolated using
584 a Percoll gradient (Genesee Scientific). Parasites were then split in two, and
585 immediately transferred to red blood cells at 1% hematocrit in warm medium without or
586 with biotin (50 μM). Both parasite cultures were incubated for 4 h at 37°C with shaking
587 to let them egress and invade new red blood cells. Cultures were then treated with 5%

588 sorbitol to remove remaining late-stage parasites. Biotinylated culture was washed in 1X
589 PBS, incubated on ice for 10 min to inactivate biotinylation and then stored at -80 °C,
590 until processing. Non-biotinylated culture was incubated for 16 h at 37°C with shaking,
591 then incubated for 4 h in medium with biotin and finally collected as previously
592 described.

593 Parasite pellets were lysed using extraction buffer (40 mM Tris-HCL pH 7.6, 150 mM
594 KCl, 1mM EDTA, 5% NP-40 and 1X HALT) and sonication (3x, 10% amplitude, 20 s
595 pulses). Streptavidin MagneSphere Paramagnetic Particle beads (Promega) were used
596 to isolate biotinylated proteins. Beads were washed three times in 1 mL of 1X PBS.
597 Protein lysates were incubated with the Streptavidin beads for 1 h at room temperature.
598 After removal of the unbound fraction, the magnetic beads were washed twice with an
599 extraction buffer and once in 1X PBS. The biotinylated proteins on the magnetic beads
600 were digested and analyzed at the Proteomics and Metabolomics shared resource at
601 Fred Hutchinson Cancer Research Center using a Orbitrap Fusion with ETD Mass
602 Spectrometer. All proteins identified in this study are in Supplemental Table 2. All mass
603 spectrometry proteomic data have been deposited to the ProteomeXchange consortium
604 via the MassIVE partner repository with the dataset identified PXD034946 (Project
605 name: Rapid proximity biotinylation of the *Plasmodium falciparum* exported protein,
606 SBP1).

607

608

609

610

611

612

613

614

615 # References

616

617 1. Organization, W. H. & Others. World malaria report 2021. (2021).

618 2. Moxon, C. A., Gibbins, M. P., McGuinness, D., Milner, D. A., Jr & Marti, M. New Insights
619 into Malaria Pathogenesis. *Annu. Rev. Pathol.* **15**, 315–343 (2020).

620 3. Ashley, E. A., Pyae Phyo, A. & Woodrow, C. J. Malaria. *Lancet* **391**, 1608–1621 (2018).

621 4. Spillman, N. J., Beck, J. R. & Goldberg, D. E. Protein export into malaria parasite-infected
622 erythrocytes: mechanisms and functional consequences. *Annu. Rev. Biochem.* **84**, 813–
623 841 (2015).

624 5. Spielmann, T. & Gilberger, T. W. Critical Steps in Protein Export of Plasmodium falciparum
625 Blood Stages. *Trends Parasitol.* **31**, 514–525 (2015).

626 6. Matthews, K. M., Pitman, E. L. & de Koning-Ward, T. F. Illuminating how malaria parasites
627 export proteins into host erythrocytes. *Cell. Microbiol.* **21**, e13009 (2019).

628 7. de Koning-Ward, T. F., Dixon, M. W. A., Tilley, L. & Gilson, P. R. Plasmodium species:
629 master renovators of their host cells. *Nat. Rev. Microbiol.* **14**, 494–507 (2016).

630 8. Maier, A. G., Cooke, B. M., Cowman, A. F. & Tilley, L. Malaria parasite proteins that
631 remodel the host erythrocyte. *Nat. Rev. Microbiol.* **7**, 341–354 (2009).

632 9. Desai, S. A. Why do malaria parasites increase host erythrocyte permeability? *Trends*
633 *Parasitol.* **30**, 151–159 (2014).

634 10. Hiller, N. L. *et al.* A host-targeting signal in virulence proteins reveals a secretome in
635 malarial infection. *Science* **306**, 1934–1937 (2004).

636 11. Marti, M., Good, R. T., Rug, M., Knuepfer, E. & Cowman, A. F. Targeting malaria virulence
637 and remodeling proteins to the host erythrocyte. *Science* **306**, 1930–1933 (2004).

638 12. Heiber, A. *et al.* Identification of new PNEPs indicates a substantial non-PEXEL exportome
639 and underpins common features in Plasmodium falciparum protein export. *PLoS Pathog.* **9**,

640 e1003546 (2013).
641 13. Blisnick, T. *et al.* Pfsbp1, a Maurer's cleft Plasmodium falciparum protein, is associated with
642 the erythrocyte skeleton. *Mol. Biochem. Parasitol.* **111**, 107–121 (2000).
643 14. Saridaki, T., Frohlich, K. S., Braun-Breton, C. & Lanzer, M. Export of PfSBP1 to the
644 Plasmodium falciparum Maurer's clefts. *Traffic* **10**, 137–152 (2009).
645 15. Maier, A. G. *et al.* Skeleton-binding protein 1 functions at the parasitophorous vacuole
646 membrane to traffic PfEMP1 to the Plasmodium falciparum-infected erythrocyte surface.
647 *Blood* **109**, 1289–1297 (2007).
648 16. Spycher, C. *et al.* MAHRP-1, a novel Plasmodium falciparum histidine-rich protein, binds
649 ferriprotoporphyrin IX and localizes to the Maurer's clefts. *J. Biol. Chem.* **278**, 35373–35383
650 (2003).
651 17. Spycher, C. *et al.* The Maurer's cleft protein MAHRP1 is essential for trafficking of PfEMP1
652 to the surface of Plasmodium falciparum-infected erythrocytes. *Mol. Microbiol.* **68**, 1300–
653 1314 (2008).
654 18. Su, X. Z. *et al.* The large diverse gene family var encodes proteins involved in
655 cytoadherence and antigenic variation of Plasmodium falciparum-infected erythrocytes. *Cell*
656 **82**, 89–100 (1995).
657 19. Baruch, D. I. *et al.* Cloning the P. falciparum gene encoding PfEMP1, a malarial variant
658 antigen and adherence receptor on the surface of parasitized human erythrocytes. *Cell* **82**,
659 77–87 (1995).
660 20. Baruch, D. I. *et al.* Identification of a region of PfEMP1 that mediates adherence of
661 Plasmodium falciparum infected erythrocytes to CD36: conserved function with variant
662 sequence. *Blood* **90**, 3766–3775 (1997).
663 21. Spielmann, T. *et al.* A cluster of ring stage-specific genes linked to a locus implicated in
664 cytoadherence in Plasmodium falciparum codes for PEXEL-negative and PEXEL-positive

665 proteins exported into the host cell. *Mol. Biol. Cell* **17**, 3613–3624 (2006).
666 22. Gruring, C. *et al.* Uncovering common principles in protein export of malaria parasites. *Cell*
667 *Host Microbe* **12**, 717–729 (2012).
668 23. Beck, J. R., Muralidharan, V., Oksman, A. & Goldberg, D. E. PTEX component HSP101
669 mediates export of diverse malaria effectors into host erythrocytes. *Nature* **511**, 592–595
670 (2014).
671 24. Elsworth, B. *et al.* PTEX is an essential nexus for protein export in malaria parasites.
672 *Nature* **511**, 587–591 (2014).
673 25. Beck, J. R. & Ho, C. M. Transport mechanisms at the malaria parasite-host cell interface.
674 *PLoS Pathog.* **17**, e1009394 (2021).
675 26. Garten, M. & Beck, J. R. Structured to conquer: transport across the Plasmodium
676 parasitophorous vacuole. *Curr. Opin. Microbiol.* **63**, 181–188 (2021).
677 27. Matthews, K. M., Kalanon, M. & de Koning-Ward, T. F. Uncoupling the Threading and
678 Unfoldase Actions of Plasmodium HSP101 Reveals Differences in Export between Soluble
679 and Insoluble Proteins. *MBio* **10**, (2019).
680 28. Gabriela, M. *et al.* A revised mechanism for how Plasmodium falciparum recruits and
681 exports proteins into its erythrocytic host cell. *PLoS Pathog.* **18**, e1009977 (2022).
682 29. Batinovic, S. *et al.* An exported protein-interacting complex involved in the trafficking of
683 virulence determinants in Plasmodium-infected erythrocytes. *Nat. Commun.* **8**, 16044
684 (2017).
685 30. Jonsdottir, T. K. *et al.* Characterisation of complexes formed by parasite proteins exported
686 into the host cell compartment of Plasmodium falciparum infected red blood cells. *Cell.*
687 *Microbiol.* **23**, e13332 (2021).
688 31. Carmo, O. M. S. *et al.* Virulence determinant, PTP7, controls vesicle budding from the
689 Maurer's clefts, adhesin protein trafficking and host cell remodeling in Plasmodium
690 falciparum. *bioRxiv* 2021.08.12.456062 (2021) doi:10.1101/2021.08.12.456062.

691 32. Takano, R. *et al.* A High-Resolution Map of SBP1 Interactomes in Plasmodium falciparum-
692 infected Erythrocytes. *iScience* **19**, 703–714 (2019).
693 33. McHugh, E. *et al.* Role of Plasmodium falciparumProtein GEXP07 in Maurer's Cleft
694 Morphology, Knob Architecture, and P. falciparumEMP1 Trafficking. *MBio* **11**, 479 (2020).
695 34. Branon, T. C. *et al.* Efficient proximity labeling in living cells and organisms with TurboID.
696 *Nat. Biotechnol.* **36**, 880–887 (2018).
697 35. May, D. G., Scott, K. L., Campos, A. R. & Roux, K. J. Comparative Application of BioID and
698 TurboID for Protein-Proximity Biotinylation. *Cells* **9**, (2020).
699 36. Nkrumah, L. J. *et al.* Efficient site-specific integration in Plasmodium falciparum
700 chromosomes mediated by mycobacteriophage Bxb1 integrase. *Nat. Methods* **3**, 615–621
701 (2006).
702 37. Mundwiler-Pachlatko, E. & Beck, H.-P. Maurer's clefts, the enigma of Plasmodium
703 falciparum. *Proc. Natl. Acad. Sci. U. S. A.* **110**, 19987–19994 (2013).
704 38. Cooke, B. M. *et al.* A Maurer's cleft-associated protein is essential for expression of the
705 major malaria virulence antigen on the surface of infected red blood cells. *J. Cell Biol.* **172**,
706 899–908 (2006).
707 39. Iriko, H. *et al.* Skeleton binding protein 1 (SBP1) of Plasmodium falciparum accumulates in
708 electron-dense material before passing through the parasitophorous vacuole membrane.
709 *Parasitol. Int.* **75**, 102003 (2020).
710 40. Dellibovi-Ragheb, T. A. *et al.* Host biotin is required for liver stage development in malaria
711 parasites. *Proceedings of the National Academy of Sciences* **115**, E2604–E2613 (2018).
712 41. Larochelle, M., Bergeron, D., Arcand, B. & Bachand, F. Proximity-dependent biotinylation
713 mediated by TurboID to identify protein-protein interaction networks in yeast. *J. Cell Sci.*
714 **132**, (2019).
715 42. Roux, K. J., Kim, D. I., Raida, M. & Burke, B. A promiscuous biotin ligase fusion protein
716 identifies proximal and interacting proteins in mammalian cells. *J. Cell Biol.* **196**, 801–810

717 (2012).
718 43. Kim, D. I. *et al.* An improved smaller biotin ligase for BioID proximity labeling. *Mol. Biol. Cell*
719 **27**, 1188–1196 (2016).
720 44. Kudyba, H. M. *et al.* The endoplasmic reticulum chaperone PfGRP170 is essential for
721 asexual development and is linked to stress response in malaria parasites. *Cell. Microbiol.*
722 **21**, e13042 (2019).
723 45. Ho, C.-M. *et al.* Malaria parasite translocon structure and mechanism of effector export.
724 *Nature* **19**, 1 (2018).
725 46. Garten, M. *et al.* EXP2 is a nutrient-permeable channel in the vacuolar membrane of
726 Plasmodium and is essential for protein export via PTEX. *Nat Microbiol* **3**, 1090–1098
727 (2018).
728 47. Charnaud, S. C., Kumarasingha, R., Bullen, H. E., Crabb, B. S. & Gilson, P. R. Knockdown
729 of the translocon protein EXP2 in Plasmodium falciparum reduces growth and protein
730 export. *PLoS One* **13**, e0204785 (2018).
731 48. Grüring, C. *et al.* Development and host cell modifications of Plasmodium falciparum blood
732 stages in four dimensions. *Nat. Commun.* **2**, 165 (2011).
733 49. McMillan, P. J. *et al.* Spatial and temporal mapping of the PfEMP1 export pathway in
734 Plasmodium falciparum. *Cell. Microbiol.* **15**, 1401–1418 (2013).
735 50. Lobingier, B. T. *et al.* An Approach to Spatiotemporally Resolve Protein Interaction
736 Networks in Living Cells. *Cell* **169**, 350–360.e12 (2017).
737 51. Mair, A., Xu, S.-L., Branon, T. C., Ting, A. Y. & Bergmann, D. C. Proximity labeling of
738 protein complexes and cell-type-specific organellar proteomes in Arabidopsis enabled by
739 TurboID. *Elife* **8**, (2019).
740 52. Santos-Barriopedro, I., van Mierlo, G. & Vermeulen, M. Off-the-shelf proximity biotinylation
741 for interaction proteomics. *Nat. Commun.* **12**, 5015 (2021).
742 53. Amos, B. *et al.* VEuPathDB: the eukaryotic pathogen, vector and host bioinformatics

743 resource center. *Nucleic Acids Res.* **50**, D898–D911 (2022).
744 54. Kono, M., Prusty, D., Parkinson, J. & Gilberger, T. W. The apicomplexan inner membrane
745 complex. *Front. Biosci.* **18**, 982–992 (2013).
746 55. Kono, M. *et al.* Evolution and architecture of the inner membrane complex in asexual and
747 sexual stages of the malaria parasite. *Mol. Biol. Evol.* **29**, 2113–2132 (2012).
748 56. Bullen, H. E. *et al.* A Novel Family of Apicomplexan Glideosome-associated Proteins with
749 an Inner Membrane-anchoring Role. *Journal of Biological Chemistry* vol. 284 25353–25363
750 (2009).
751 57. Rajaram, K., Liu, H. B. & Prigge, S. T. Redesigned TetR-Aptamer System To Control Gene
752 Expression in Plasmodium falciparum. *mSphere* **5**, (2020).
753 58. de Koning-Ward, T. F. *et al.* A newly discovered protein export machine in malaria
754 parasites. *Nature* **459**, 945–949 (2009).
755 59. Maier, A. G. *et al.* Exported proteins required for virulence and rigidity of Plasmodium
756 falciparum-infected human erythrocytes. *Cell* **134**, 48–61 (2008).
757 60. Vincensini, L. *et al.* Proteomic analysis identifies novel proteins of the Maurer's clefts, a
758 secretory compartment delivering Plasmodium falciparum proteins to the surface of its host
759 cell. *Mol. Cell. Proteomics* **4**, 582–593 (2005).
760 61. Das, S., Basu, H., Korde, R., Tewari, R. & Sharma, S. Arrest of nuclear division in
761 Plasmodium through blockage of erythrocyte surface exposed ribosomal protein P2. *PLoS*
762 *Pathog.* **8**, e1002858 (2012).
763 62. Muralidharan, V., Oksman, A., Pal, P., Lindquist, S. & Goldberg, D. E. Plasmodium
764 falciparum heat shock protein 110 stabilizes the asparagine repeat-rich parasite proteome
765 during malarial fevers. *Nat. Commun.* **3**, 1310 (2012).
766 63. Birnbaum, J. *et al.* A genetic system to study Plasmodium falciparum protein function. *Nat.*
767 *Methods* **14**, 450–456 (2017).
768 64. Araiso, Y., Imai, K. & Endo, T. Role of the TOM Complex in Protein Import into

769 Mitochondria: Structural Views. *Annu. Rev. Biochem.* **91**, 679–703 (2022).

770 65. Lamb, I. M. *et al.* Mitochondrially targeted proximity biotinylation and proteomic analysis in
771 Plasmodium falciparum. *bioRxiv* 2022.05.30.494025 (2022)
772 doi:10.1101/2022.05.30.494025.

773 66. Claros, M. G. & Vincens, P. Computational method to predict mitochondrially imported
774 proteins and their targeting sequences. *Eur. J. Biochem.* **241**, 779–786 (1996).

775 67. Cobb, D. W. *et al.* The Exported Chaperone PfHsp70x Is Dispensable for the Plasmodium
776 falciparum Intraerythrocytic Life Cycle. *mSphere* **2**, e00363–17 (2017).

777 68. Zimbres, F. M. *et al.* Metabolomics profiling reveals new aspects of dolichol biosynthesis in
778 Plasmodium falciparum. *Sci. Rep.* **10**, 401 (2020).

779 69. Kudyba, H. M., Cobb, D. W., Florentin, A., Krakowiak, M. & Muralidharan, V. CRISPR/Cas9
780 Gene Editing to Make Conditional Mutants of Human Malaria Parasite P. falciparum. *J. Vis.*
781 *Exp.* 1–10 (2018).

782 70. Ganesan, S. M. *et al.* Yeast dihydroorotate dehydrogenase as a new selectable marker for
783 Plasmodium falciparum transfection. *Mol. Biochem. Parasitol.* **177**, 29–34 (2011).

784
785
786
787
788
789
790
791
792
793
794
795
796
797
798
799
800

801
802
803
804
805
806
807
808
809
810
811
812
813 **SUPPLEMENTAL FIGURES**

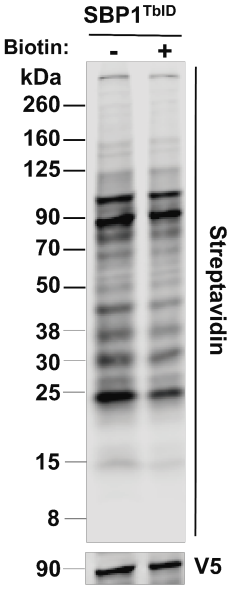

814

815 **Supplemental figure 1. Biotinylation of proximal proteins by TurboID$_{V5}$-tagged SBP1**.
816 Western blot of parasite lysates isolated from the mutant line SBP1^{TbID} grown in complete RPMI
817 medium, incubated with or without biotin (50 μM) for 2 h. Samples were probed with antibodies
818 against V5 (loading control) and fluorescent dye-labeled streptavidin. The protein marker sizes
819 are shown on the left.

820

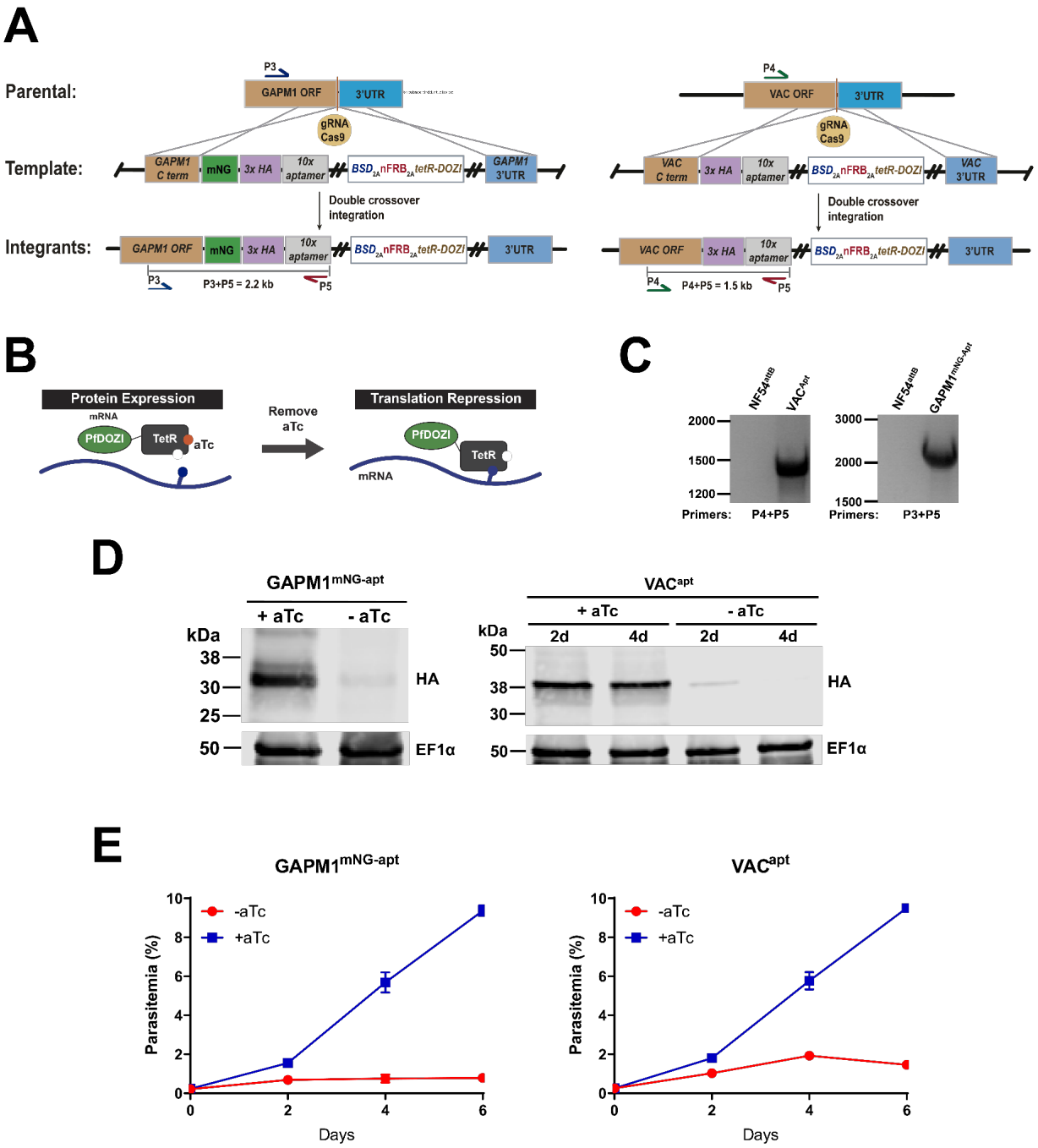

Supplemental figure 2. Characterization of parasite lines VAC^{apt} and GAPM1$^{mNG\text{-}apt}$. (A) Schematic showing the integration of the repair plasmid to modify the genomic loci of Pf3D7_1432100 (VAC) and Pf3D7_1323700 (GAPM1). Cas9 introduces a double-stranded break at the C-terminus of the VAC and GAPM1 locus. The repair plasmid provides homology regions for double-crossover homologous recombination, introducing the HA-tag and the TetR-Aptamer system. For GAPM1$^{mNG\text{-}apt}$, a fluorescent tag mNeonGreen was introduced between the C-terminus and the HA-tag. (B) Regulation of protein expression using the TetR-Aptamer knockdown system. TetR binds to aptamer repeats in the mRNA, while PfDOZI localizes the

complex to sites of mRNA sequestration, causing a repression in translation of the gene of interest. Anhydrous tetracycline (aTc) binds to TetR, blocking its interaction with the aptamers. (A) PCR test confirming integration at the VAC and GAPM1 locus. Amplicons were amplified from genomic DNA isolated from mutant and wild-type parasites. Primers were designed to amplify the region between the C-terminus and the tandem of 10X aptamer repeats. (B) Western blot of parasite lysates isolated from the mutant lines VAC^{apt} and GAPM1$^{mNG\text{-}apt}$ probed with antibodies against HA and EF1α (loading control). The protein marker sizes are shown on the left. GAPM1$^{mNG\text{-}apt}$ parasites were collected after incubation for 48 h in the presence or absence of aTc. VAC^{apt} parasites were collected after incubation for 48 and 96 h in presence or absence of aTc. (C) Growth of synchronous VAC^{apt} and GAPM1$^{mNG\text{-}apt}$ parasites over 6 days after removal of aTc from the medium via flow cytometry. Representative of three biological replicates shown for each growth curve. Each data point represents the mean of three technical replicates; error bars represent standard deviation.

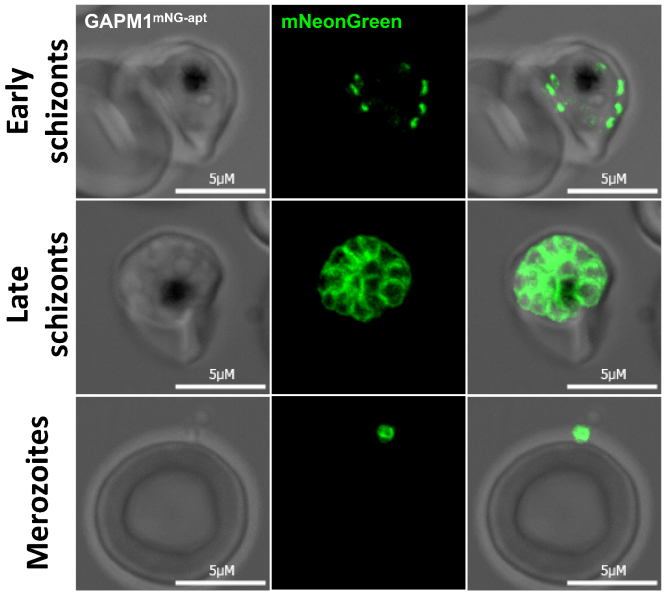

Supplemental figure 3. Localization of GAPM1 at late stages in the GAPM1$^{mNG\text{-}apt}$ cell line. (A) Representative live images showing GAPM1$^{mNG\text{-}apt}$ localization at early and late schizonts, and merozoites. Images of GAPM1$^{mNG\text{-}apt}$ from left to right are phase-contrast, mNeonGreen (green), and fluorescence merge. Z stack images were deconvolved and projected as a combined single image.

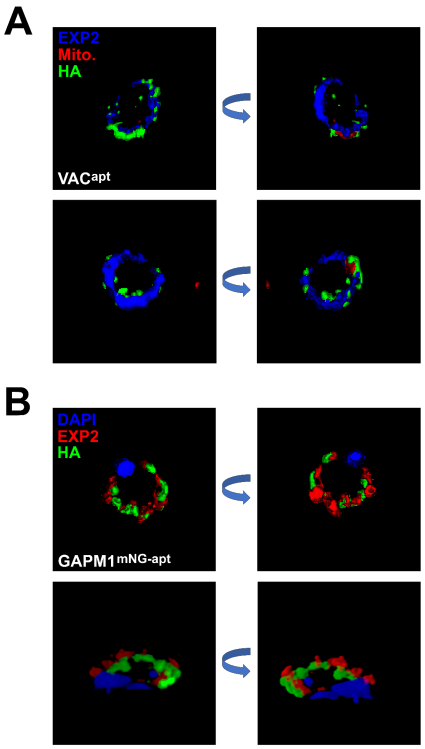

856

857 **Supplemental figure 4. Localization of VAC and GAPM1 at early stage parasites.** 3D
858 reconstruction based on structured illumination microscopy images captured from (A) VAC^{apt}
859 and (B) GAPM1$^{mNG\text{-}apt}$ ring-stage parasites at 4 hpi and stained with the antibodies as in Fig 5A.

860
861
862
863
864
865
866 **Supplemental Table 1.** List of primers used in the study to generate the cell lines SBP1^{TbID},
867 VAC^{apt} and GAPM1$^{mNG\text{-}apt}$
868
869
870 **Supplemental Table 2.** Complete list of proteins identified using label-free analysis and
871 collected by mass spectrometry.